RSC Advances




ROYAL SOCIETY OF CHEMISTRY

www.rsc.org/advances

Cite this: DOI: 10.1039/c0xx00000x

www.rsc.org/xxxxxx

Full paper

# Flexible Quantum Dot Light Emitting Diode Based on ZnO Nanoparticles

**Jiangyong Pan[a] , Jing Chen [*a], Qianqian Huang[a] , Qasim Khan[a] , Xiang Liu[a] , Zhi Tao [a], Wei Lei[*a], Feng Xu [a], Zichen Zhang[*b]**

***Received (in XXX, XXX) Xth XXXXXXXXX 20XX, Accepted Xth XXXXXXXXX 20XX***
**DOI: 10.1039/b000000x**

Flexible quantum dot light emitting diodes (QLEDs) have attracted extensive attention owing to the advantages of foldability and their broad application in flexible display devices. In this work, we reported on the high performance, mechanically flexible QLEDs based on ZnO nanoparticles used as electron transfer layer (ETL). The QLEDs have been fabricated over poly (ethylene-terephthalate) (PET) substrates utilizing a unique structure consisting of bilayered hole transport films and ZnO nanoparticles were acted as ETL to improve the device performance owing to its proper energy band position and high charge mobility. The QLEDs exhibited high performance of lowered turn on voltage of 1.6 V, and improved current and power efficiency of 5.20 cd/A and 1.80 lm/W, respectively. It is represented the good flexibility with a critical bending radius of 4.5 mm, suggesting the broad application prospect of flexible QLEDs.

## 1. Introduction

Colloidal quantum dots (QDs) are considered as the rising candidate for the new-generation light-emitting materials because it possesses unique properties of the tunable emission wavelengths because of quantum confinement effect, highly saturated emission color, narrow emission with small full width at half maxima (FWHM), solution processed, and compatible with flexible substrates.[1, 2] Since the first report of electrically driven quantum dot LEDs (QLEDs) utilizing CdSe QDs in 1994,[3] QLEDs have received considerable attention for academic research and potential commercialization. After about two decades of research and development, QLEDs are reaching the performance of organic LEDs (OLEDs) and emerging as a candidate for single-material, full-color light sources. [4-7] It is noted that in the past few years, much effort has been made to improve the efficiency of QLED by optimization of active materials and employment of novel structures. For example, in the review report, Reineke S. has summarized the major structures improvement of QDs such as the adoption of a core–shell configuration, the passivation of surface trap states, and the engineering of the electronic and chemical properties of the organic ligands surrounding the QDs and mentioned the major superiority of QLEDs over OLED in the spectral purity. [8] Yang et al. have demonstrated a full series of blue, green and red QLEDs with high efficiencies, which can be achieved by optimizing nanostructure of quantum dots, especially the composition of the graded intermediate shell and the thickness of the outer shell. [9] As for the employment of novel structure, Dai et al. have reported highly efficient QLED by inserting an insulating layer between the quantum dot layer and the oxide electron-transport layer to optimize charge balance in the device. [6] In addition, Charles W et al. demonstrated the surface plasmon-enhanced EL in QLEDs by incorporating Au NPs in the ZnO electron transport layer, which provide strong coupling between localized surface plasmon (LSPs) in Au NPs and excitons in QDs.[10]

Despite much progress in the improvement of device performance, QLEDs are still faced with many problems, especially low stability including drastic efficiency roll-off at high current densities and low operational lifetime,[6] lower electroluminescence (EL) efficiency compared with those of OLEDs due to the limitations in electrical properties and the device structure[11] and high production cost due to the use of vacuum-requiring thermal evaporation. [8]

Most investigated devices have been fabricated on rigid substrates, such as glasses up to now.[11, 12] Flexibility is one of the key elements for the future information display,[13, 14] especially in the intelligent household electrical appliance. The key advantages of flexible electronics, compared with current silicon technologies, are low-cost manufacturing and inexpensive flexible substrates through the use of roll-to-roll (or sheet-to-sheet) fabrication methods with high yield and high throughput. Recently, Yang et al. have reported highly efficient, large-area QLED tapes emitting in full color with top-emitting design and polyimide tapes as flexible substrates.[7] Panzer et al. have demonstrated the tunable infrared emission from printed colloidal quantum dot/polymer composite films on flexible substrates. The display operates by optical down conversion of AC-driven blue phosphor electroluminescence using different-sized, IR-emitting colloidal quantum dots.[15] In addition, Yohan et al. demonstrated the QLEDs using InP/ZnSe/ZnS multi shell colloidal QDs prepared by simple heating-up synthesis, which was fabricated on polyethylene naphthalate (PEN) substrate for flexible

optoelectronic device.[16] However, the optoelectronic properties of QLEDs on the flexible substrate are not fully investigated yet and it is also faced with many problems such as high turn on voltage, low device efficiency and instability.

In this work, we report the flexible QLEDs, which have been designed and fabricated over indium tin oxide (ITO)-coated polyethylene terephthalate (PET) substrates. The adoption of 2.9 nm-sized ZnO NPs as ETL and dual HTL in the structure is to balance the charge transfer rate. The lowered turn on voltage of 1.6 eV, improving efficiency of 5.20 cd/A and enhanced stability (lifetime of more than 100 hours without encapsulation) can be archived for the flexible QLED. Meanwhile, it is found that the critical bending radius is 4.5 mm for this type of flexible QLED.

## 2. Experimental section

**Chemicals.** Cadmium oxide (CdO, 99.99%), zinc acetate (99.9%, powder), selenium (99.9%, powder), sulfur (99.9%, powder), trioctylphosphine (TOP, 90%), oleic acid (OA, 90%), 1-octadecene (ODE, 90%), zinc acetate (99.9%, powder), dimethyl sulphoxide (reagent grade, 99%), tetramethyl-ammonium hydroxide (99.99%, powder) were used as purchased from Aldrich.

**Synthesis of Quantum Dots**

Green emitting ZnCdSeS QDs were synthesized according to a modified method reported previously.[17] Here, 0.4 mmol of CdO, 4 mmol of zinc acetate, 4 mmol of oleic acid (OA), and 20 mL of 1-octadecne were mixed in a 100 mL round flask. The mixture was heated to 150 °C degassed under ~10 pa pressure for 30 min, filled with high-purity $N_2$ flowing, and further heated to 300 °C to form a clear solution of $Cd(OA)_2$ and $Zn(OA)_2$. At this temperature, a stock solution containing 3 ml of trioctylphosphine, 0.4 mmol of Se, and 4 mmol of S was quickly injected into the reaction flask. After the injection, the reaction temperature was maintained for 10 min to promote the growth of QDs. The reaction was subsequently cooled down to room temperature to stop further growth. The QDs were washed with acetone three times, and finally dispersed in toluene at a concentration of 10 mg/ml.

**Synthesis of ZnO NPs**

The ZnO NPs were synthesized through a solution-precipitation process using Zn acetate and tetramethylammonium hydroxide (TMAH) precursors. The reaction process is present as followed: A solution of 0.5 M tetramethylammonium hydroxide (TMAH) in ethanol and 0.1 M zinc acetate in dimethyl sulphoxide (DMSO) were mixed and stirred for 1 hour in ambient atmosphere[18]. The prepared product was collected by centrifugation and then washed. The obtained transparent precipitate was dispersed in butanol at a concentration of 30 mg/ml. A $TiO_2$ sol–gel precursor (DuPont tyzol BTP) was diluted to 5 wt% in butanol to be used as ETL in QLEDs for comparison.

QLEDs were fabricated on poly (ethylene-terephthalate) (PET) substrates covered with indium tin oxide (ITO). The substrates were firstly cleaned with de-ionized water, acetone and iso-propanol, consecutively, for 15 min each, and then treated with ultraviolet light ozone for half an hour to increase the work function and modify the surface energy of ITO. Poly (ethylenedioxythiophene): poly styrenesulphonate (PEDOT: PSS) solutions (filtered through a 0.22 mm filter) were spin-coated onto the ITO/PET flexible substrates at 5000 r.p.m. for 30 s and baked at 120 ℃ for 20 min under ambient conditions. The PEDOT: PSS-coated flexible substrates were transferred into a nitrogen-filled glove box ($O_2$ < 0.1 p.p.m., $H_2O$ < 0.1 p.p.m.) for spin-coated the sequential layers. The poly (N,N9-bis(4-butylphenyl)-N,N9-bis(phenyl)-benzidine) (Poly-TPD) used as the hole transport layer (1 wt% in chlorobenzene) was spin-coated at 2500 r.p.m for 30 s, followed by baking at 110℃ for 30 min. After that, poly(9-vinlycarbazole) (PVK) (2 mg/ml in toluene) was deposited at 2500 r.p.m for 30 s and QDs (10 mg/ml in toluene) layers at 800 r.p.m for 30 s followed by baking at 120 ℃ for 15 min. Then the ZnO NPs (30 mg/ml in butanol) were spin coated at 4000 r.p.m for 30 s and baked at 120℃. The thicknesses of PEDOT: PSS, poly-TPD, PVK, ZnCdSeS QD and ZnO NPs are 30 nm, 30 nm, 5 nm, 28 nm, and 30 nm, respectively. The size of QD and the thickness of ZnO and QD layer in the QLED has been optimized. (Fig. S1, Supporting Information) Finally, the top Al cathode was deposited in a custom high-vacuum deposition chamber (background pressure, $6\times10^{-4}$ torr) with an active device area of 120 $mm^2$.

The morphology and size information of the ZnO NPs was analyzed using a Cs-corrected high-resolution transmission electron microscope (HRTEM, Tecnai G20). The current-voltage (I-V) characteristics were measured with a Keithley-2400 source-meter unit. The absorption spectra was measured using U-4100 UV-visible. The luminance of the devices was calibrated using a Minolta luminance meter (LS-100).

## 3. Results and discussion

The structure and schematic energy band diagram of the QLED is shown in Fig. 1(a) and Fig. 1(b), respectively. Here, the multilayer device consists of layers of PET/ ITO/ PEDOT:PSS (30 nm)/ Poly-TPD (30 nm)/ PVK (5 nm)/ ZnCdSeS QD (28 nm)/ ZnO NPs (30 nm)/Al, in which PEDOT: PSS used as the hole injection layer (HIL), poly-TPD and PVK as the hole transport layer (HTL), ZnCdSeS QD as the emission layer (EML), and ZnO NPs for electron transport layer (ETL). The size of QD is about 7.5 nm (Fig. S2, Supporting Information).The photoluminescent quantum yields (PL QY) of the QDs were measured and estimated of 60% by comparing their fluorescence intensities with those of primary standard dye solutions (Rhodamine 6G, QY=95% in ethanol) at the same optical density (0.05) at the same excitation wavelength (370 nm). In addition, relatively uniform surface morphologies of compactly packed ZnO NP layers by spin-coating process can be seen from SEM images(Fig. S3, Supporting Information). The schematic energy level diagram of the device depicted in Fig. 1(b) shows that the electrons can easily be injected from the Al to the QD layer and holes can be restricted within QD layer stemming from the electron affinity of ~3.7 eV and ionization potential of ~7.3 eV for ZnO NPs (Fig. S4, Supporting Information). Thus, the ZnO NPs layer can confine the excitation-recombination region hence potentially improving the efficiency of charge recombination. However, the case is different for the hole injection. The hole is difficult to transport from hole injection layer PEDOT: PSS to QD layer owing to the relative larger energy barrier of ~1 eV between HOMO of PEDOT: PSS and valance band of QD. As a



 

result, the bilayered hole transport films of poly-TPD and PVK are adopted to decrease the energy barrier between adjacent layers for holes transport and increase the injection force of holes, further to balance the electron and hole injection. In addition, the cross-sectional SEM image of QLED is shown as in Fig. 1(c). It can be clearly seen from the figure that the device consists layers of ITO /PEDOT:PSS/ Poly-TPD /PVK/QD/ZnO/Al. The thickness of PEDOT:PSS, Poly-TPD /PVK, QD, ZnO and Al is estimated about 30 nm, 36 nm, 30 nm, 30 nm and 120 nm respectively, which is good agreement with the statistic results from the step profiler. It is noted that the PVK layer is hardly distinguished from the SEM image because its thickness is rather small.

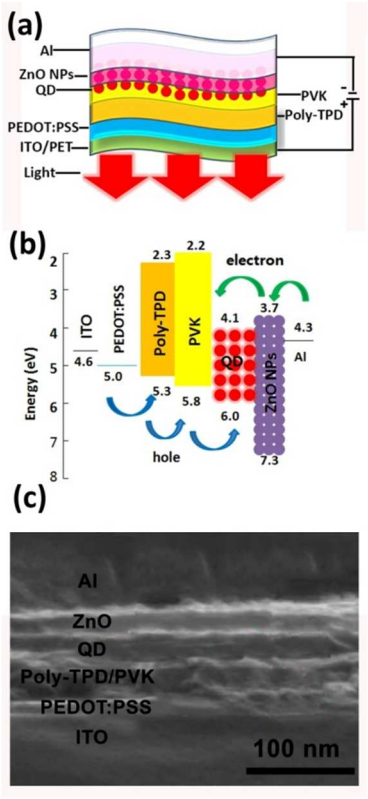


**Fig. 1** (a) Structure and (b) energy level diagram for the various layers of QLEDs (c) SEM image of the cross section of QLED

A high-resolution transmission electron microscope (HRTEM) image of the ZnO NPs is displayed in Fig. 2(a) and (b), and inset shows the statistical distribution images of particle size, indicating that the ZnO NPs have an average diameter of ~2.9 nm. Lattice fringes can be clearly observed in the HRTEM image which suggests good crystallinity of the ZnO NPs in Fig. 2(b). Fig. 2(c) shows the XRD pattern of ZnO NPs film. It can be seen from the figure that our synthesized ZnO NPs has wurtzite structure, which is in good agreement with the literature values (JCPDS card no. 79-0207), although the small particle size led to a significant broadening of the characteristic diffraction. It is shown the absorption and photoluminescence spectra of ZnO NPs in Fig. 2(d). It is observed that the peak position of absorption was located at 320 nm. The band gap $E_g$ of the colloidal ZnO NPs is determined from the intercept between the wavelength axis and the tangent to the linear section of the absorption band edge.[19] The band gap is 3.65 eV for the 2.9 nm NPs, which is higher than that of bulk ZnO (3.2–3.3 eV), [20] indicating that there is higher spatial confinement of photo-generated charge carriers in the smaller ZnO particles.[21] From the photoluminescence spectra, we observe two peaks in the PL spectra. The intensity of one peak is relatively weak and located at the fundamental absorption band edge of the NP. This can be attributed to the direct electron–hole recombination. [22] The other peak is much more intense and is located at 500–550 nm, reflecting radiative recombination of electrons and holes, involving traps or structural defects on the surface of the NPs.[23]

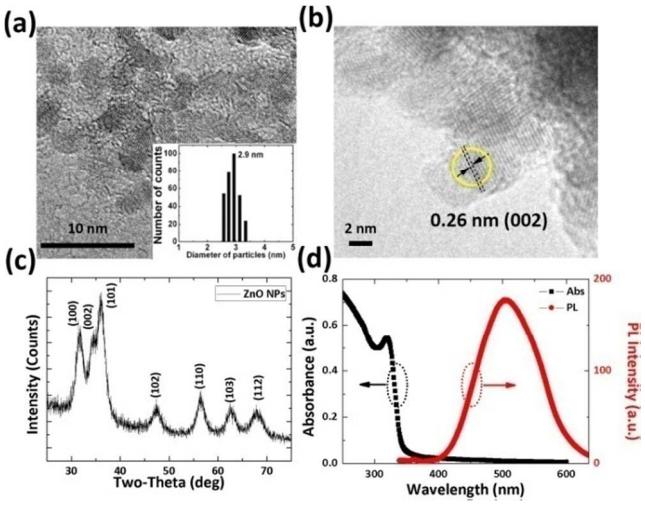


**Fig. 2** (a)TEM image of ZnO NPs. Inset shows the statistical distribution images of particle size (b) HRTEM image of ZnO NPs (c) XRD pattern from ZnO NPs film (d) Absorption and photoluminescence spectra of ZnO NPs.

Fig. 3(a) and (b) shows a comparison of the electrical properties and device performance of the QLEDs based on ZnO NPs ETL and $TiO_2$ ETL, respectively.

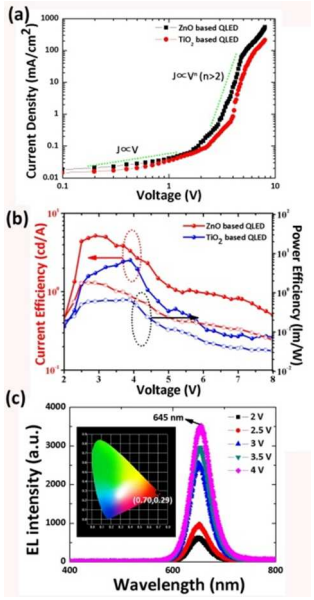


**Fig. 3** (a) Current density versus voltage characteristics of the QLED, (b) current efficiency and power efficiency of the QLED (c) EL spectra of ZnO-based QLED as the applied voltage varying from 2-4 V. Inset shows the CIE coordinate of device emitting

From Fig. 3(a), It can be seen the slope of the current density–voltage (J–V) curve showed ohmic behavior ($J \propto V$) at low voltage region for the both devices. It changed to present trap-limited conduction ($J \propto V^n$, $n>2$) as the operating voltage increased. The trap-limited conduction maintained beyond the turn-on voltage, suggesting that the QDs acted as trap sites in the devices.[24]

Compared to the $TiO_2$-based QLED, the ZnO-based QLED gives larger current density over the entire voltage range, which can be concluded that the ability of electron injection and transport through ZnO NPs is superior to that of $TiO_2$ in our device structure. It is mainly due to the much higher electron mobility of ZnO NPs ($4.8\times10^{-3}$ $cm^2/V\cdot s$) (Fig. S5, Supporting Information) than that of amorphous $TiO_2$ ($\sim1.0\times10^{-4}$ $cm^2/V\cdot s$).[25] Meanwhile, the turn-on voltage (driving voltage corresponding to a luminance of 0.1 cd $m^{-2}$) of QLED based on ZnO NPs was also significantly decreased to 1.6 V, which was lowered than that of the $TiO_2$-based device (2.5 V).

Reduced turn-on driving voltages for the QLED are expected to lead to higher efficiency and better device stability, as Fig. 3(b) depicted. The ZnO-based QLED shows higher current and power efficiency over the entire driving voltage. And the maximum current efficiency and power efficiency are 5.20 cd/A, 1.80 lm/W for ZnO-based QLED and 2.54 cd/A, 0.94 lm/W for $TiO_2$ based QLED respectively. The lowered turn-on voltage and higher efficiency for ZnO based QLED is attributed to the Auger-assisted charge injection[4]. In our system, during this process, the holes can be easily injected to PVK because of the existence of Poly-TPD, which decreases the energy barrier between adjacent layers for holes transport and increase the injection force of holes as shown in Fig. 1(b). These holes accumulate at the PVK/QD interface due to the energy offset (~0.2 eV) between the HOMO level of PVK and the valence band (VB) edge of the QD. Similarly, electrons can be easily injected to the QD because of large electron mobility of $4.8\times10^{-3}$ $cm^2/V\cdot s$ in ZnO and small energy barrier of 0.6 eV between QD and Al. However, the energy offset of ~1.9 eV between the LUMO of PVK and the conduction band (CB) of QD leads to electron accumulation at the PVK/QD interface. In other words, the injected holes and electrons from electrodes are likely to accumulate at the interface between PVK and the QDs due to the large energy barrier offset. Once the Auger assisted hole injection process takes place, where one high energy hole can be obtained after absorbing the energy released from the interfacial recombination of an electron–hole pair.[26] The high-energy holes can go over the injection barrier at PVK/QD interface and recombine with electrons inside the QD layer and emit photons.[27] It schematically illustrates the sequence of the Auger-like energy up-conversion process occurring at the heterojunction interface in Fig. S6, Supporting Information. It is demonstrated that the process is proportional to the electron injection level.[18] In other words, the process is more easily to take place under the condition of more electron injection from cathode. Thus, $TiO_2$ based devices do not exhibit a low turn on voltage from Auger-assisted charge injection because of its low electron mobility of $1\times10^{-4}$ $cm^2/V\cdot s$[25]. In contrast, electrons can be efficiently injected into a ZnO NPs-based device at low voltages by the Auger process, which is attributed to the higher electron mobility of $4.8\times10^{-3}$ $cm^2/V\cdot s$ in spite of proper band alignments in both devices. In addition, the good performance of ZnO-based QLED is also attributed to the design of Poly-TPD/PVK bilayered hole transport structure in the device, which can facilitate the hole transport and balance the carrier injection, thus increase the device performance. Moreover, in order to deeply understand the operating mechanism of different ETL-based devices, we further analyzed the voltage–efficiency characteristics at low operation voltages for the two ETL-based devices. For ZnO based devices, it can be seen that maximum efficiencies can be reached at rather low voltage (less than 3 V), much faster than that based on $TiO_2$ device (nearly 4 V). In addition, it shows a rise of current efficiency for $TiO_2$-based devices as the voltage increases from 2 to 4 V. The rise can be explained as part of the QDs in an initial (darkened) negatively charged state due to the relatively larger barrier between HTL and QD and an excess of electrons in the QD region results in QD charging. The amount of holes injection into QDs layer increases as the voltage increases (current density), which consequently decreases the probability of QD charging and enhances the device efficiency.[28] In contrast, an Auger assisted energy up conversion hole injection occurs at the PVK/QD interface in the ZnO-based device due to the high electron mobility of the ZnO NPs layer, which leads to an efficient hole injection into the QD layer at low voltage, thus balance the holes and electrons. As a result, high efficiency can be achieved for ZnO-based device at a lower current density.

The EL spectrum of QLED under different voltage is shown in Fig. 3(c). The intensity increases with increasing applied voltage. It can be seen that the position of the EL peak is located at 645 nm. The peak wavelength is red-shifted of 12 nm compared with that of the photoluminescence (PL) peak of QD solution (Fig. S2, Supporting Information) stemming from a combination of finite dot-to-dot interactions in close-packed solid films and the electric-field-induced Stark effect.[29] The inset shows the device emitting corresponds with the CIE coordinate of (0.70, 0.29).

In order to study the lifetime of the device, the luminance versus time for an unencapsulated red QLED under ambient conditions was measured at a constant voltage of 4 V and current density of 8 $mA/cm^2$ shown as Fig. 4.

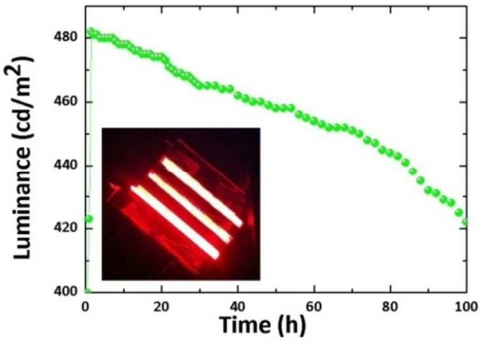


**Fig. 4** Stability data for an unencapsulated ZnO-based QLED. Inset shows the real photo of the QLED

The luminance is initially 423 $cd/m^2$ and increases quickly to 482 $cd/m^2$ within few hours, which is consistent with the trend from the previously report.[27, 30] Then the luminance intensity decreases very slowly during the next 100 hours. It is easy to find

that the lifetime (operating time corresponding to half of the initial luminance) exceeds 100 h. The inset of Fig. 4 shows the photo of the flexible prototype of the ZnO-based QLED under driving voltage of 4 V. The red emitting light is very dazzling and high saturation with the corresponding CIE coordinate of (0.70, 0.29). The current ZnO-based QLEDs show considerable stability under ambient conditions, because the ZnO layer not only helps to facilitate the electron transport but also served as a barrier against diffusion of oxygen and water molecule into the active layers.

In addition to the good opt-electrical performance, the distinct advantages of our devices are their highly flexible and mechanically robust structure. The QLED can be easily bent into almost any three-dimensional shape with PET substrates, which facilitates the versatile use of our QLED platform. Its robustness is confirmed by the bending test of devices with bending radius varying from 3 to 12 mm shown in Fig. 5. In order to obtain different bending radius of device, the flexible device is placed and bent around different curvature of steel plate, shown in inset of Fig. 5. The figure depicts that the brightness intensity remains about 75% after being bent 300 times under the bending radius of 3 mm or 4 mm, whereas the brightness changes slightly after being bent 300 times with bending radius larger than 4.5 mm.

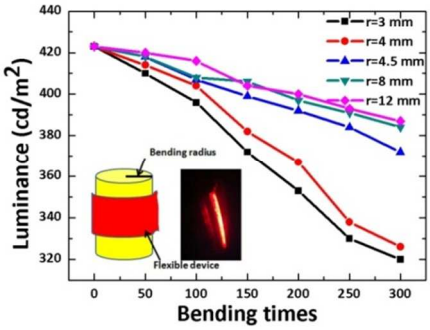


**Fig. 5** Bending testing of flexible ZnO-based QLED. Inset shows the schematic diagram and corresponding electroluminance picture of the device with bending radius of 3 mm after 300 times bending

In order to research the performance deterioration of devices after bending test and find out the critical bending radius, the current density-voltage and efficiency-voltage characterization of the device bent into different states of curvature were displayed in Fig. 6 (a) and (b), respectively.

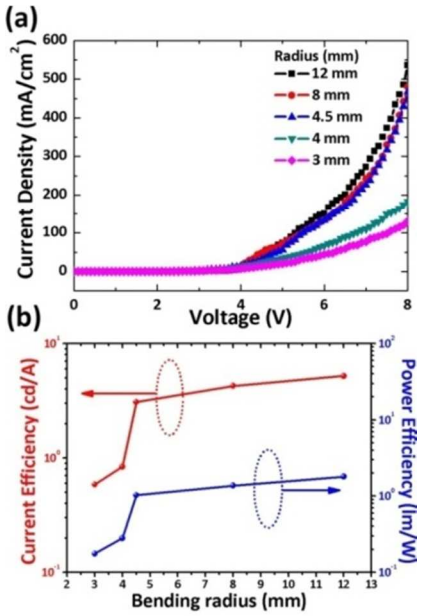


**Fig. 6** (a) Current density versus voltage characteristics of the QLED (b) maximum current efficiency and power efficiency of the QLED under bending conduction

It is found that the current density variation trend is similar when bending radius is larger than 4.5 mm, which is similar to the condition for the device efficiency. Fig. 6(b) depicts that the current and power efficiency both decrease quickly once the bending radius is smaller than 4.5 nm, which suggests that the critical radius is 4.5 mm. The poor performance of device under small bending radius conduction is attributed to the onset of the cracking phenomenon in the ITO films, because the molecular components in the LED device are highly compressible.[31] Table 1 summarizes the detailed performance parameters of the QLEDs of different bending radius in the present study. The small critical bending radius suggests that flexible QLED has broad prospect in the application of large, conformable, or roll-up flat panel displays. In addition, the flexible QLED-based displays have advantage in fabricating cost because it can be mass manufactured on a roll-to-roll basis owing to its good flexibility.

**Table 1** Summary of luminance loss, current density at 6V (C-D), power efficiency $\eta_P$ and current efficiency $\eta_A$ of QLEDs based on different bending radius.

| Bending radius (mm) | Luminance loss (%) | C-D (mA/cm$^2$) | $\eta_P$ (lm W$^{-1}$) | $\eta_A$ (cd A$^{-1}$) |
|---|---|---|---|---|
| 3 | 24.3 | 44.53 | 0.18 | 0.59 |
| 4 | 22.9 | 67.15 | 0.28 | 0.84 |
| 4.5 | 12.1 | 133.40 | 1.03 | 3.09 |
| 8 | 9.2 | 134.02 | 1.37 | 4.26 |
| 12 | 8.5 | 142.27 | 1.67 | 5.09 |

## 4. Conclusions

In summary, we designed and fabricated flexible red-emitting QLEDs on ITO/PET substrates using ZnO NPs as ETL, which displays low turn on voltage, high current and power efficiency of 1.60 V, 5.20 cd/A and 1.80 lm/W respectively. The better performance is owing to the higher electron mobility of ZnO NPs and more suitable energy level of bilayered HTL consisting of

poly-TPD/PVK. Moreover, the lifetime of more than 100 h for the unencapsulated flexible device under ambient conditions has been achieved. Finally, the flexible QLEDs exhibit a critical bending radius down to 4.5 mm, which is useful for their applications in flexible display and roll to roll manufacture. Our work paves the way for realizing all solution processed flexible QLED and presents the broad prospect of flexible QD optoelectronics.

## Acknowledgments

This work was supported partially by the National Key Basic Research Program 973 (2013CB328804, 2013CB328803), the National High-Tech R&D Program 863 of China (2012AA03A302, 2013AA011004), National Natural Science Foundation Project (51120125001, 61271053, 61306140, 61405033, 91333118, 61372030, and 51202028), and Natural Science Foundation Project of Jiangsu Province (BK20141390, BK20130629, and BK20130618).

## Notes and references

[a]*School of Electronic Science and Engineering, Southeast University, Nanjing, China, 210096;E-mail:chenjing@seu.edu.cn; lw@seu.edu.cn*
[b] *State Key Laboratory of Precision Measurement Technology and Instruments, Department of Precision Instrument, Tsinghua University, Beijing 100084, China ;E-mail: zz241@tsinghua.edu.cn*

† Electronic Supplementary Information (ESI) available: [Optimized procedure of the QLED fabrication, Characteristic of the QD, Characteristic of the ZnO NP film, Illustration of the Auger-like energy up-conversion process, UPS measurements, UV-Vis absorption spectrum for ZnO film, TFT characteristics of ZnO nanoparticle film]. See DOI: 10.1039/b000000x/

1. Shirasaki, Y.; Supran, G. J.; Bawendi, M. G.; Bulovic, V. *Nat. Photonics* **2013,** 7, 13-23.
2. Sun, Q.; Wang, Y. A.; Li, L. S.; Wang, D.; Zhu, T.; Xu, J.; Yang, C.; Li, Y. *Nat. Photonics* **2007,** 1, 717-722.
3. Colvin, V. L.; Schlamp, M. C.; Alivisatos, A. P. *Nature* **1994,** 370, 354-357.
4. Qian, L.; Zheng, Y.; Xue, J. G.; Holloway, P. H. *Nat. Photonics* **2011,** 5, 543-548.
5. Shirasaki, Y.; Supran, G. J.; Bawendi, M. G.; Bulović, V. *Nat. Photonics* **2013,** 7, 13-23.
6. Dai, X.; Zhang, Z.; Jin, Y.; Niu, Y.; Cao, H.; Liang, X.; Chen, L.; Wang, J.; Peng, X. *Nature* **2014,** 515, 96-99.
7. Yang, X. Y.; Mutlugun, E.; Dang, C.; Dev, K.; Gao, Y.; Tan, S. T.; Sun, X. W.; Demir, H. V. *Acs Nano* **2014,** 8, 8224-8231.
8. Reineke, S. *Nat Mater* **2015,** 14, 459-462.
9. Yang, Y.; Zheng, Y.; Cao, W.; Titov, A.; Hyvonen, J.; MandersJesse, R.; Xue, J.; Holloway, P. H.; Qian, L. *Nat Photon* **2015,** 9, 259-266.
10. Kim, N. Y.; Hong, S. H.; Kang, J. W.; Myoung, N.; Yim, S. Y.; Jung, S.; Lee, K.; Tu, C. W.; Park, S. J. *Rsc Advances* **2015,** 5, (25), 19624-19629.
11. Kwak, J.; Bae, W. K.; Lee, D.; Park, I.; Lim, J.; Park, M.; Cho, H.; Woo, H.; Yoon, D. Y.; Char, K.; Lee, S.; Lee, C. *Nano Lett.* **2012,** 12, 2362-2366.
12. Lim, J.; Bae, W. K.; Lee, D.; Nam, M. K.; Jung, J.; Lee, C.; Char, K.; Lee, S. *Chem. Mater.* **2011,** 23, 4459-4463.
13. Tan, Z. N.; Xu, J.; Zhang, C. F.; Zhu, T.; Zhang, F.; Hedrick, B.; Pickering, S.; Wu, J.; Su, H. P.; Gao, S.; Wang, A. Y.; Kimball, B.; Ruzyllo, J.; Dellas, N. S.; Mohney, S. E. *Journal of Applied Physics* **2009,** 105, (3).
14. Liang, R. Z.; Yan, D. P.; Tian, R.; Yu, X. J.; Shi, W. Y.; Li, C. Y.; Wei, M.; Evans, D. G.; Duan, X. *Chem. Mater.* **2014,** 26, 2595-2600.
15. Panzer, M. J.; Wood, V.; Geyer, S. M.; Bawendi, M. G.; Bulovic, V. *J. Disp. Technol.* **2010,** 6, 90-93.
16. Kim, Y.; Greco, T.; Ippen, C.; Wedel, A.; Oh, M. S.; Han, C. J.; Kim, J. *Nanosci. Nanotechnol. Lett.* **2013,** 5, 1065-1069.
17. Bae, W. K.; Char, K.; Hur, H.; Lee, S. *Chem. Mater.* **2008,** 20, 531 - 539.
18. Qian, L.; Zheng, Y.; Choudhury, K. R.; Bera, D.; So, F.; Xue, J. G.; Holloway, P. H. *Nano Today* **2010,** 5, 384-389.
19. Panasiuk, Y. V.; Raevskaya, O. E.; Stroyuk, O. L.; Kuchmiy, S. Y.; Dzhagan, V. M.; Hietschold, M.; Zahn, D. R. T. *Nanotechnology* **2014,** 25.
20. Ozgur, U.; Alivov, Y. I.; Liu, C.; Teke, A.; Reshchikov, M. A.; Dogan, S.; Avrutin, V.; Cho, S. J.; Morkoc, H. *J. Appl. Phys.* **2005,** 98.
21 Kamat, P. V.; Patrick, B. *J. Phys. Chem.* **1992,** 96, 6829-6834.
22. Stroyuk, O. L.; Dzhagan, V. M.; Shvalagin, V. V.; Kuchmiy, S. Y. *J. Phys. Chem. C* **2010,** 114, 220-225.
23. Spanhel, L.; Anderson, M. A. *J. Am. Chem. Soc.* **1991,** 113, 2826-2833.
24. Hikmet, R.; Talapin, D.; Weller, H. *J. Appl. Phys.* **2003,** 93, 3509-3514.
25. Kim, J. Y.; Kim, S. H.; Lee, H. H.; Lee, K.; Ma, W. L.; Gong, X.; Heeger, A. J. *Adv. Mater.* **2006,** 18, 572-+.
26. Demir, H. V.; Nizamoglu, S.; Erdem, T.; Mutlugun, E.; Gaponik, N.; Eychmuller, A. *Nano Today* **2011,** 6, (6), 632-647.
27. Qasim, K.; Chen, J.; Li, Z.; Lei, W.; Xa, J. *RSC Adv.* **2013,** 3, 12104-12108.
28. Xu, W.; Ji, W. Y.; Jing, P. T.; Yuan, X.; Wang, Y. A.; Xiang, W. D.; Zhao, J. L. *Opt. Lett.* **2014,** 39, 426-429.
29. Kim, H. H.; Park, S.; Yi, Y.; Son, D. I.; Park, C.; Hwang, D. K.; Choi, W. K. *Sci. Rep.* **2015,** 5, 5.
30. Chen, J.; Zhao, D.; Li, C.; Xu, F.; Lei, W.; Sun, L.; Nathan, A.; Sun, X. W. *Sci. Rep.* **2014,** 4.
31. Gu, G.; Burrows, P.; Venkatesh, S.; Forrest, S.; Thompson, M. *Opt. Lett.* **1997,** 22, 172-174.



 